ENERGY STORAGE

10.1126/sciadv.1500886

High–energy density nonaqueous all redox flow lithium battery enabled with a polymeric membrane

Chuankun Jia,[1] Feng Pan,[1] Yun Guang Zhu,[1] Qizhao Huang,[1] Li Lu,[2] Qing Wang[1]*

Redox flow batteries (RFBs) are considered one of the most promising large-scale energy storage technologies. However, conventional RFBs suffer from low energy density due to the low solubility of the active materials in electrolyte. On the basis of the redox targeting reactions of battery materials, the redox flow lithium battery (RFLB) demonstrated in this report presents a disruptive approach to drastically enhancing the energy density of flow batteries. With $LiFePO_4$ and TiO_2 as the cathodic and anodic Li storage materials, respectively, the tank energy density of RFLB could reach ~500 watt-hours per liter (50% porosity), which is 10 times higher than that of a vanadium redox flow battery. The cell exhibits good electrochemical performance under a prolonged cycling test. Our prototype RFLB full cell paves the way toward the development of a new generation of flow batteries for large-scale energy storage.

INTRODUCTION

Large-scale electrochemical energy storage has long been regarded as an important means to enhance the efficiency and power quality of the electrical grid by effective peak shaving and valley filling. This has become more pressingly important when a large amount of energy generated by instable and intermittent renewable power sources is connected to the grid in the context of growing environmental concerns and limited fossil fuel reserves. Redox flow batteries (RFBs) are considered one of the most promising electrochemical energy storage technologies because of their decoupled energy storage and power generation, which leads to a flexible system design, greater safety, and a long cycle life (*1*–*3*). However, the large-scale deployment of RFB systems is largely hampered by low energy density, a result of low volumetric capacity and cell voltage. For instance, the energy density of the most developed all-vanadium redox flow battery (VRB) is only $^1/_{10}$ that of lithium-ion batteries, innately restricted by the solubility of vanadium-based redox species and the narrow electrochemical window of aqueous electrolyte (*4*, *5*). Although the former has been addressed in some "hybrid" redox flow systems, issues pertaining to the poor cycling performance of the metal electrode and challenges of achieving a good balance between ionic conductivity and crossover of the membrane remain (*6*).

Although nonaqueous RFBs are far less developed than aqueous RFBs, they have recently received considerable attention because of the broader electrochemical window of the organic solvents and the availability of a wide range of redox mediators. As summarized in Fig. 1, nonaqueous electrolyte systems based on metallocene (*7*), metal-bipyridyl complexes (*8*), metal-acetylacetonate complexes (*9*–*11*), and metal-free organic redox molecules (*12*) have recently been extensively explored, which demonstrated much higher voltage than their aqueous counterpart (*13*–*15*). However, the low solubility of these redox species in nonaqueous solvent (usually much lower than 1 M) becomes a major obstacle to achieving higher energy density. Some high-concentration nonaqueous redox electrolytes in alkaline metal–based hybrid flow systems have been recently reported, such as Li-I, Li-Fc, Li-TEMPO (2,2,6,6-tetramethylpiperidine-1-oxyl), and Li/MTLT (4-methoxy-2,2,6,6-tetramethylpiperidine 1-oxyl and lithium bis(trifluoromethanesulfonyl) imide) ionic liquid flow cells (*16*–*19*). Again, the cycling stability of lithium metal upon repeated plating and stripping remains unsolved. The use of semisolid flow batteries is an alternative approach to addressing the above problems by pumping slurries of solid active materials through the cells (*20*–*24*). However, its practical application may be limited by the low utilization ratio of the active materials and the high viscosity of the fluids. In this regard, on the basis of the "redox targeting" concept, we have recently proposed a conceptually new approach—RFLB, which stores energy in lithium-ion battery materials while operating as an RFB—to address the above issues. Compared with the semisolid flow battery, the solid materials of RFLB are statically kept in the two tanks, whereas the energy is reversibly stored and released through chemical lithiation/delithiation reactions mediated by the redox species dissolved in electrolyte. Because nonaqueous electrolyte is used and energy is stored in the condensed state, in which $[Li^+]$ is generally larger than 20 M, the energy density is thus drastically enhanced.

In our previous studies, we have demonstrated RFLB half-cells using $LiFePO_4$ (*25*) and TiO_2 (*26*) as the Li storage material. Combining the two half-cells would, in principle, lead to an RFLB full cell, without using the labile lithium metal. Although it seems intuitive to proceed with this, there arises the challenge of a robust Li^+-conducting membrane being critically required for the operation of RFLB full cells. In the case of half-flow cells, as the Li metal in the anodic compartment is passivated by a solid-electrolyte interphase layer, it could effectively block the self-discharge caused by the crossover of the redox mediator, but not in the case of RFLB full cells. Hence, a mechanically and chemically stable membrane that is impermeable to redox mediators and with high Li^+ conductivity is desired for the operation of RFLBs. However, the commonly used glass ceramic membranes such as OHARA LICGC (lithium ion–conducting glass-ceramics) or LATP $[Li_{1+x}Al_xTi_{2-x}(PO_4)_3]$ are chemically instable in the reductive anolyte (*27*, *28*). In addition, the ceramic membranes are prone to break because of their poor mechanical stability. In contrast, although polymeric membranes, especially

[1]Department of Materials Science and Engineering, Faculty of Engineering, National University of Singapore, Singapore 117576, Singapore. [2]Department of Mechanical Engineering, Faculty of Engineering, National University of Singapore, Singapore 117576, Singapore.
*Corresponding author. E-mail: msewq@nus.edu.sg

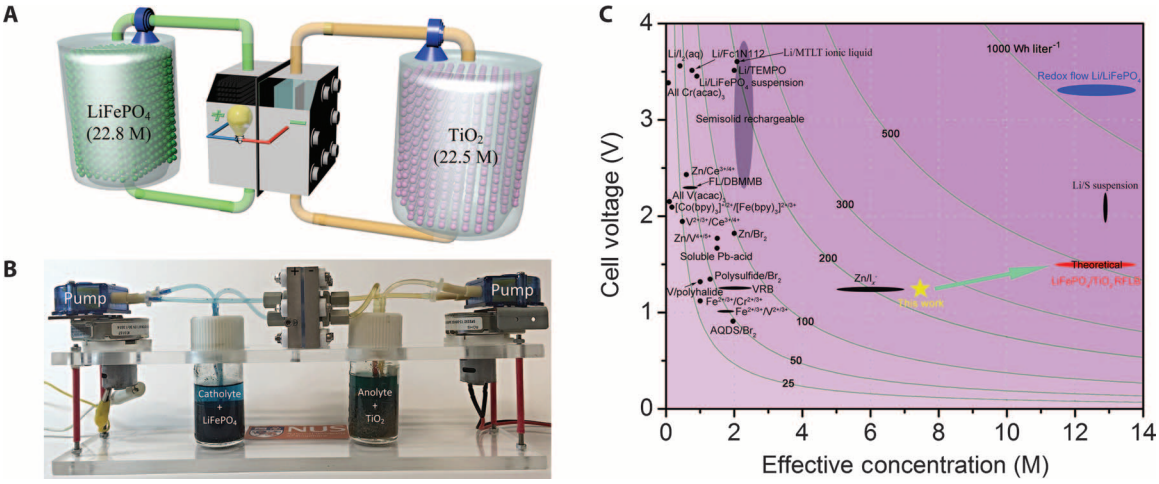

Fig. 1. Concept of an RFLB full cell and a summary of the reported energy density of various aqueous and nonaqueous RFBs. (**A**) Schematic illustration of a redox flow lithium battery (RFLB) full cell. It has two separate tanks filled with porous $LiFePO_4$ and TiO_2 granules. Catholyte and anolyte are circulated through the materials in the tanks and to the cell during charging and discharging. (**B**) Photograph of an RFLB full cell used in this report. Electrolytes are circulated with two peristaltic pumps. (**C**) A plot summarizing various flow-type battery chemistries in terms of cell voltage, effective concentration of redox species (by considering the number of electrons involved in the reaction), and energy density.

those based on Nafion (commonly used in aqueous RFBs), have good flexibility and chemical stability, their performance is greatly compromised in nonaqueous RFBs due to the high permeability of redox mediators. Therefore, a suitable membrane is needed for the development of RFLB full cells. Here, we report a polymeric Nafion/polyvinylidene difluoride (PVDF) composite membrane that enables the operation of the first RFLB full cell. As shown in Fig. 1, granules of $LiFePO_4$ and TiO_2, which are used as the cathodic and anodic Li storage materials, respectively, are statically kept in two separate tanks in the full cell. Two pairs of redox mediators, namely, dibromoferrocene ($FcBr_2$) and ferrocene (Fc), and cobaltocene [$Co(Cp)_2$] and bis(pentamethylcyclopentadienyl)cobalt [$Co(Cp^*)_2$], are used in the catholyte and anolyte for the redox targeting reactions with $LiFePO_4$ and TiO_2, respectively. Because of the condensed state of the materials, the Li^+ concentration in $LiFePO_4$ and TiO_2 is 22.8 and 22.5 M (for $Li_{0.5}TiO_2$), which amounts to a theoretical volumetric capacity of 613 and 603 ampere-hours per liter (Ah liter^{-1}), respectively (*29*). Considering a 50% porosity of the materials in the tank, the reachable tank energy density of an RFLB full cell could be as high as ~500 watt-hours per liter (Wh liter^{-1}), which is 10 times that of the conventional VRB (50 Wh liter^{-1} for one tank) (*30*). We anticipate that RFLB will pave the way for next-generation large-scale energy storage.

RESULTS

Physical properties of the Nafion/PVDF membrane

An ideal membrane has high areal Li^+ conductivity, minimum redox mediator permeability, and good mechanical strength. LISICON (lithium super ionic conductor) structured glass ceramic is a popular option in various redox flow lithium half-cells. However, the presence of Ti^{4+} makes the membrane liable to be reduced by the redox molecules in the anolyte. For instance, as shown in the inset of Fig. 2A, the OHARA LICGC glass ceramic membrane undergoes a striking color change when it is in contact with the reduced $Co(Cp^*)_2$ molecules. Moreover, the ceramic membrane is too fragile to be used as the separator in large flow cells. On the other hand, although the lithiated Nafion membrane is chemically stable with the anolyte, it suffers from severe crossover of redox mediators as a result of strong swelling induced by the electrolyte solvent (table S1), and the cell fails to be charged/discharged properly (fig. S1). Hence, here, we propose using PVDF as a rigid framework for Nafion to control the swelling and consequently eliminate the crossover. The as-prepared dry membrane NP11 (Nafion/PVDF weight ratio, 1:1) has large areal resistance, which drastically drops after it is assembled into an RFLB full cell with electrolyte circulating for 48 hours (fig. S2). The membrane "activation" process continues upon cycling the cell—a further decrease of the membrane resistance was observed after charging/discharging the cell for 47 cycles (Fig. 2A). In contrast to the glass ceramic membrane, the Nafion/PVDF composite membrane presented nearly no color change after cycling, indicating good chemical stability.

The bright and dark areas in the atomic force microscopy (AFM) phase images in Fig. 2B represent the hard hydrophobic and soft hydrophilic regions of the NP11 membrane, respectively (*31*, *32*). Clearly, the hydrophilic -SO_3Li groups on the side chain of the Nafion membrane are uniformly interconnected with the hydrophobic fluorocarbon backbones of PVDF and Nafion, and thus, continuous Li^+ transport channels are formed. Such a microstructure of the NP11 membrane is distinct from the pure Nafion membrane (fig. S3)—the bright area corresponding to the C-F chains becomes more predominant in the composite membrane and the hydrophilic channels are surrounded by large hydrophobic domains. As a result, the swelling of the composite membrane is greatly reduced (table S1), which is further substantiated by the crossover test of the redox mediators in fig. S4. The scanning electron microscopy image in fig. S5 shows that the surface of the NP11 membrane is uniform and smooth with no crack observed. The EDX elemental mapping reveals a uniform distribution of all the four elements, corroborating the excellent dispersion of the two phases in the composite membrane. Hence, the microstructure of the NP11 membrane ensures continuous Li^+ transport through the isolated hydrophilic domains while eliminating crossover of the redox mediators with the surrounding rigid hydrophobic domains. While varying the Nafion/PVDF ratio in the composite membrane, we observed that the degree

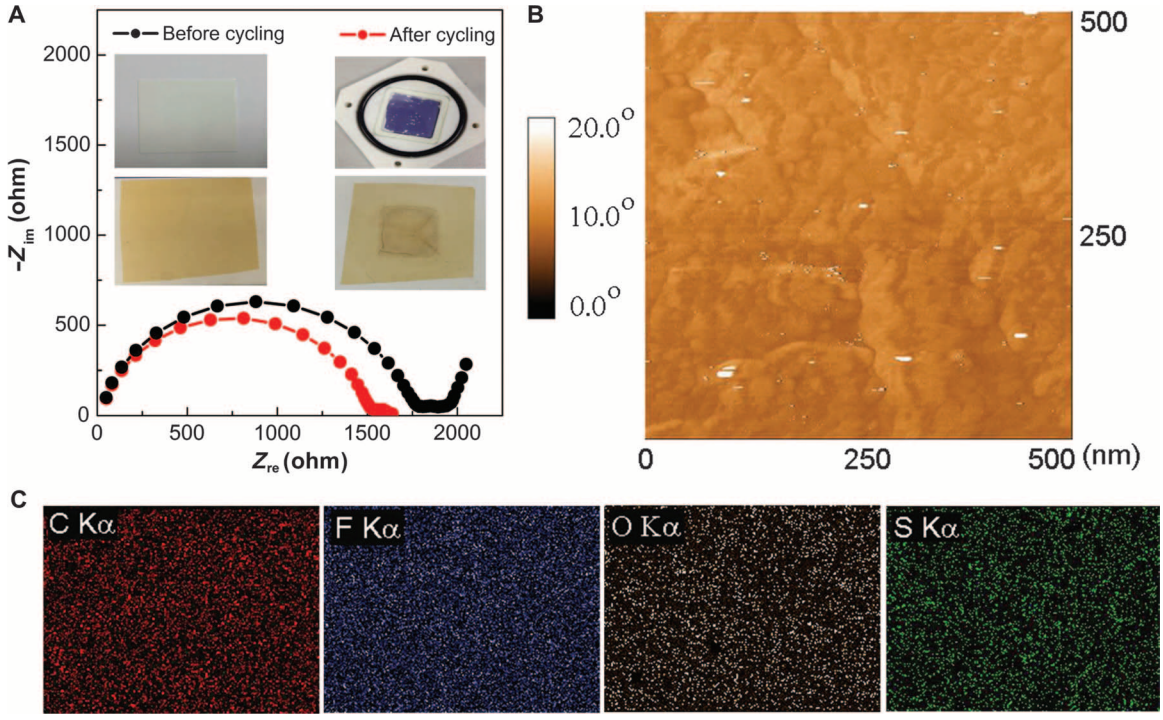

Fig. 2. General properties of Nafion/PVDF membranes. (**A**) Impedance Nyquist plots of the NP11 membrane before and after testing in an RFLB full cell for 47 cycles. The inset also shows the photographs of an OHARA LICGC and NP11 membrane before and after cycling. (**B** and **C**) AFM phase image (B) and energy-dispersive x-ray spectroscopy (EDX) elemental mapping (C) of the as-prepared NP11 membrane.

of lithiation (DL) increases with Nafion content (table S2) and so does Li^+ conductivity. Compared with the NP11 membrane, although NP21 exhibits lower areal resistance, it has severe crossover of redox mediators (fig. S4), so it can't be used in an RFLB full cell (fig. S6). In contrast, although the NP12 membrane has no crossover problem, it suffers from unendurably high areal resistance (fig. S7).

The stability of the NP11 membrane was extensively evaluated after cycling in an RFLB full cell. As shown in fig. S5B, the surface of the NP11 membrane remains smooth and uniform and no obvious changes could be observed. In addition, the distribution of S and O elements is uniform, indicating that there is no phase separation of Nafion and PVDF. Moreover, the AFM phase images (fig. S8) show that the hydrophilic -SO_3Li groups (dark area) on the side chain of the Nafion membrane remain uniformly interconnected with the hydrophobic fluorocarbon backbones (bright area) of PVDF and Nafion after cycling. Fourier transform infrared spectroscopy (FTIR) spectra further confirm the chemical stability of the NP11 membrane upon prolonged cycling. The characteristic vibration bands of Nafion and PVDF in NP11 appear the same before and after cycling in an RFLB full cell (fig. S9), suggesting excellent chemical robustness of the materials. The above characterizations unambiguously reveal that both the Nafion and PVDF components in the composite membrane retain uniform dispersion without appreciable phase separation and chemical degradation after prolonged cycling in an RFLB full cell.

RFLB full cell performance

For reversible redox targeting reactions and consequently effective energy storage in the solid active materials in the tanks to be realized, the potentials of redox mediators should just straddle those of the active materials in the same electrolyte, which thus could be reversibly oxidized (delithiated) by a mediator with a high potential and reduced (lithiated) by a mediator with a low potential. As shown in the cyclic voltammograms in Fig. 3A, the potential of $LiFePO_4$ is 3.45 V (versus Li/Li^+) on the cathodic side, which lies in between the potentials of $FcBr_2$ (3.78 V) and Fc (3.40 V). Similarly, on the anodic side, the potential of TiO_2 (~1.80 V) lies in between the potentials of $Co(Cp)_2$ (2.10 V) and $Co(Cp^*)_2$ (1.67 V).

Figure 4A shows the typical voltage profiles of an RFLB full cell, in which it used 5 mM $Co(Cp)_2/Co(Cp^*)_2$ and 5 mM $FcBr_2/Fc$ in the anolyte and catholyte, respectively. We used a slight excess quantity of TiO_2 in the anodic tank over $LiFePO_4$ in the cathodic tank to determine the reaction yield of $LiFePO_4$. Three consecutive plateaus are observed for the charging process. The first plateau at 1.80 V is determined by the oxidation of Fc in the cathodic compartment and the concurrent reduction of $Co(Cp)_2^+$ in the anodic compartment [reaction (5), Fig. 3B] when the IR drop [~0.55 V, see the galvanostatic intermittent titration technique (GITT) in Fig. 4A] across the membrane and electrolytes is taken into account. With the progress of the charging process, $Co(Cp^*)_2^+$ is subsequently reduced in the anodic side when that of $Co(Cp)_2^+$ ceases. Meanwhile, Fc continues to be oxidized on the cathodic side presumably due to the superior reaction reversibility of Fc to $Co(Cp)_2^+$, and the overall reaction reduces to reaction (3), rendering the second plateau at 2.25 V. $FcBr_2$ then starts to be oxidized when all Fc is converted to Fc^+, which leads to reaction (1), corresponding to the third plateau at 2.65 V. With the formation of $Co(Cp^*)_2$, TiO_2 starts to be lithiated as a result of redox targeting reaction between the two in the anodic storage tank, which regenerates $Co(Cp^*)_2^+$. Concomitantly, the oxidation of $FcBr_2$, forming $FcBr_2^+$, leads to the delithiation of $LiFePO_4$ in the cathodic

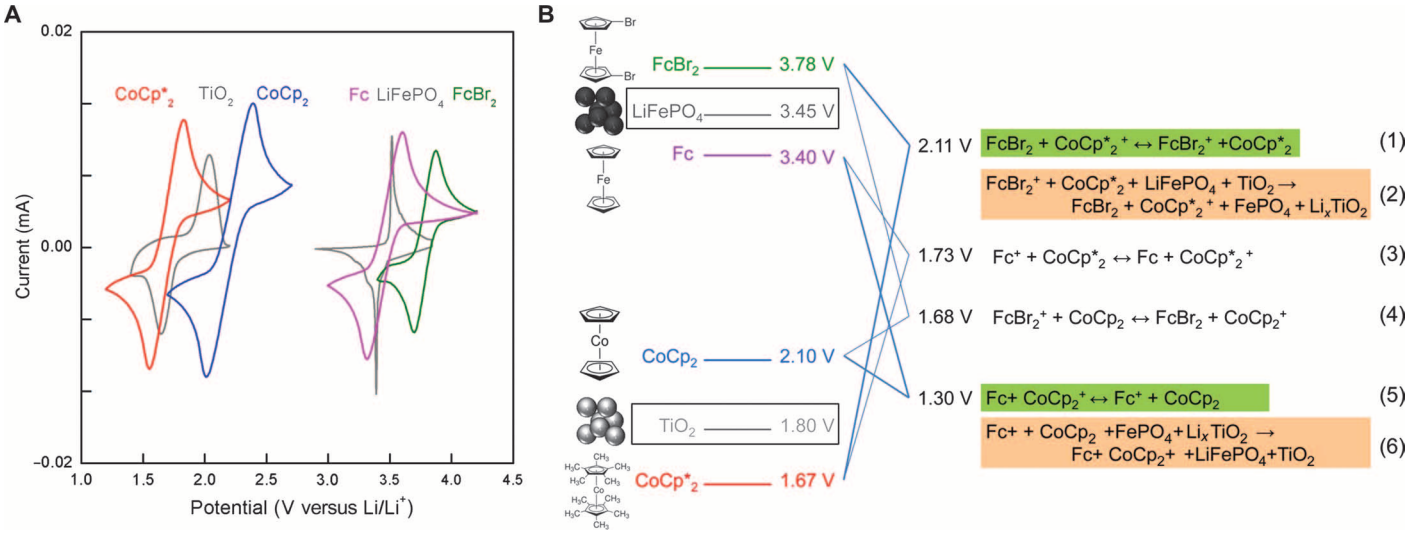

Fig. 3. Working principle of the redox targeting reactions in cathodic and anodic tanks. (**A**) Cyclic voltammograms of the redox mediators and Li storage materials—$LiFePO_4$ and TiO_2. (**B**) A scheme compiling the chemical reactions between the redox mediators and materials in the tanks, as well as the electrochemical reactions of the mediators in the cell at different charging and discharging stages.

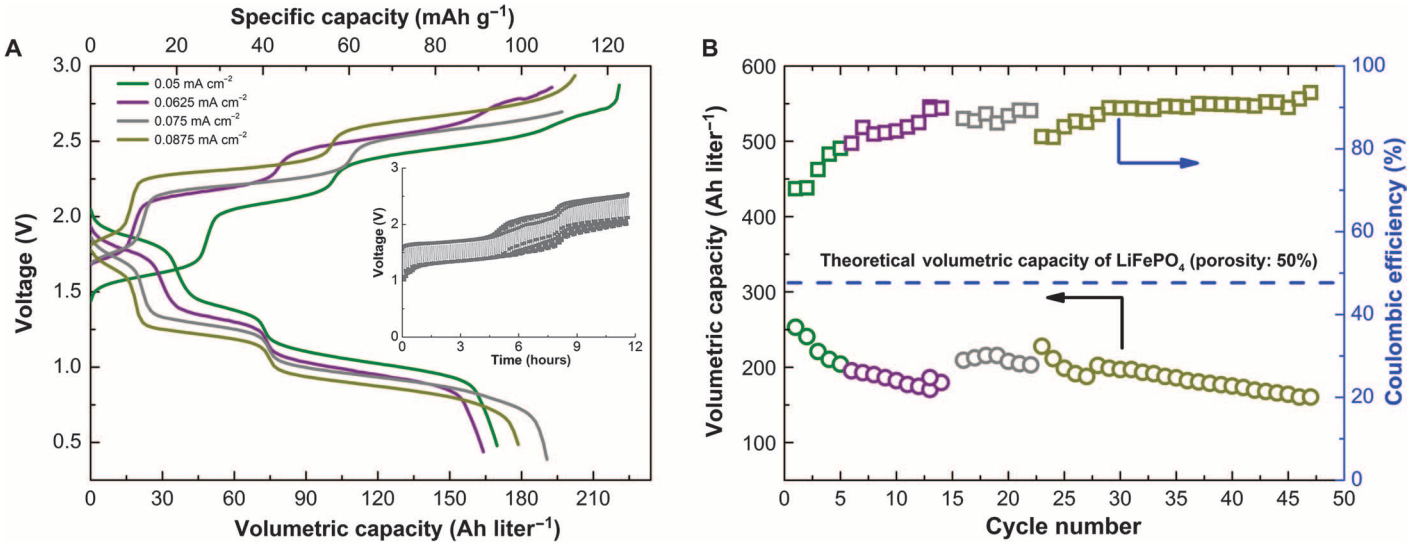

Fig. 4. Electrochemical performance of the RFLB full cell. (**A**) Typical voltage profiles of the RFLB full cell at different current densities. The inset shows a fraction of the GITT curve of the cell during the charging process at a current density of 0.05 mA cm^{-2}. (**B**) Volumetric capacity retention and coulombic efficiency of the cell over cycling at different current densities.

storage tank. As a result, the third charging plateau is obviously prolonged, and the capacities of both $LiFePO_4$ and TiO_2 are released at this stage [reaction (2)]. In contrast, only two plateaus are observed in the first charging process (fig. S10) because both $Co(Cp)_2$ and $Co(Cp^*)_2$ are initially in reduced states, and hence, reaction (5) is absent during the first charging. The discharging process nearly reverses the above electrochemical and chemical reactions with three voltage plateaus from high to low voltage corresponding to reactions (1), (4), and (5), respectively. The prolonged third plateau of the discharging curve involves the reactions of both $FePO_4$ and Li_xTiO_2 with Fc and $Co(Cp)_2$ [reaction (6)], respectively.

There is a clear trend that the voltage plateaus increase with current density. As discussed previously, the operation of RFLB relies on the chemical reactions between redox mediators and Li storage materials in the tanks, the electrochemical reactions of the redox mediators in the electrochemical cell, and the mass transport of Li^+ and redox mediators between the two, as well as that of Li^+ across the membrane. Although the microstructure of the Li storage materials in the tank is optimized, our previous study discloses that the pseudo–first-order volumetric rate constants of the Li^+-coupled heterogeneous electron transfer between $Fc/FcBr_2$ and $LiFePO_4$ are in the range of 1 to 6 s^{-1}, which is translated into a "C-rate" of more than 43C, a rather fast process for normal battery operation (*33*). In addition, as the redox mediators used here are highly reversible, the fast electrode reactions of these redox species are unlikely to dictate the power of the cell. Hence, the mass transport, especially that of Li^+ across the membrane, would plausibly

be the rate-limiting step considering that electrolyte circulation would effectively accelerate the transport of redox species and Li^+ between the tanks and the cell.

We further scrutinized the electrochemical behavior of RFLB using GITT measurement. The voltage recorded under open-circuit conditions essentially excluded the overpotential resulting from the IR drop across the membrane and electrolyte, as well as that of interfacial electron transfer on the electrodes (*34*). As shown in the inset of Fig. 4A, the recorded open-circuit voltage is reasonably consistent with the potential differences of redox molecules at various stages of reactions. The sharp voltage drop of the GITT curve at each open-circuit intermittency reveals that the overpotential largely originated from the IR drop arising from Li^+ transport across the membrane, which is in good agreement with the impedance measurement of the membrane. Thus, a substantial improvement in the Li^+ conductivity of the membrane is desirable to enhance the power output of the RFLB.

Figure 4B shows the capacity and coulombic efficiency of the RFLB full cell. The capacity remains relatively stable upon cycling (see also the voltage profiles in fig. S10B). On the basis of the mass of $LiFePO_4$, the initial charging capacity of the active species in the cathodic tank is calculated to be 135 mAh g^{-1} at 0.05 mA cm^{-2}, which is even higher than that of $LiFePO_4$ measured in a Swagelok cell (~120 mAh g^{-1}) and is six times higher than that of VRB. Considering a 50% porosity of the materials in the tank, it translates to a volumetric capacity of 243 Ah $liter^{-1}$, which is almost five times higher than that of VRB. The excellent gravimetric and volumetric capacities stem from the remarkable Li^+ concentration in the solid Li storage materials (22.8 M for $LiFePO_4$ and 22.5 M for $Li_{0.5}TiO_2$), which are very much higher than those attainable in liquid solution. Assuming a unity reaction yield for both redox mediators, we estimate the utilization ratio of $LiFePO_4$ to be 44.0 and 35.5% in the charging and discharging process, respectively, which is expected to be considerably enhanced by optimizing the packing and microstructures of $LiFePO_4$ granules in the tank. Considering an average discharging voltage of ~1.25 V at 0.075 mA cm^{-2}, the volumetric energy density of RFLB is about 238 Wh $liter^{-1}$, which is nearly five times that of VRB (50 Wh $liter^{-1}$ for one tank). We noted that the concentration of redox species in both the catholyte and anolyte is only 5 mM, which would be much higher in a practical RFLB system, thus further boosting the overall energy density of the system. Although it is striking, the tank energy density is still far from the theoretically reachable value, ~500 Wh $liter^{-1}$ (Fig. 1C), because of the nonideal redox molecules for both $LiFePO_4$ and TiO_2. For instance, the inevitable voltage loss between $LiFePO_4$ and $FcBr_2$ is 0.33 V in the charging process, and that between TiO_2 and $Co(Cp)_2$ is 0.35 V in the discharging process (Fig. 3B), considerably impairing the energy density and energy efficiency of the cell.

DISCUSSION

The above results have unambiguously demonstrated the operation of RFLB full cells using a Li^+-conducting Nafion/PVDF composite membrane. We have achieved a strikingly high energy density, being five times higher than that of VRB, when the cell used $LiFePO_4$ and TiO_2 as the cathodic and anodic Li storage materials, respectively. In addition, owing to the excellent capability of the membrane to block the crossover of redox molecules, the cell presented good cycling performance. This report suggests that the use of solid materials with dense Li^+ storage in the tank, with relatively low-concentration redox molecules mediating the reactions in the electrolyte, is a promising approach to developing high–energy density flow batteries. However, for practical applications, one must further improve the conductivity of the Li^+-conducting Nafion/PVDF membrane. In addition, the redox molecules used here are far from being ideal, which leads to intolerably large overpotential loss when they react with $LiFePO_4$ and TiO_2. It is anticipated that with a good Li^+-conducting membrane and suitable redox mediators, the full development of RFLB would provide a disruptive solution toward achieving high–energy density large-scale electrochemical storage.

MATERIALS AND METHODS

Materials

Tetraethylene glycol dimethyl ether (TEGDME, 99%, Sigma-Aldrich), lithium bis(trifluoromethane)sulfonimide (LiTFSI, Sigma-Aldrich), Fc (Sigma-Aldrich), $FcBr_2$ (TCI), $Co(Cp)_2$ (Sigma-Aldrich), $Co(Cp^*)_2$ (Sigma-Aldrich), $LiFePO_4$ (Li-Cell), and TiO_2 (Degussa, P25) were used as received. PVDF was purchased from Alfar Aesar, and Nafion 212 membrane was purchased from Ion Power Inc.

Preparation of the Nafion/PVDF membrane

The Nafion 212 membrane and PVDF powder were first heated at 70°C for 48 hours. The resulting dried Nafion 212 membrane was cut into small pieces, 175 mg of which was added into 5 ml of *N*,*N*′-dimethylformamide. The mixture was stirred vigorously and heated at 60°C to dissolve the Nafion. After the Nafion was fully dissolved, the solution was cooled to room temperature. Then, 175 mg of the dried PVDF powder was added into the above solution. The mixture was then stirred at room temperature for 4 hours to dissolve the PVDF powder. After the PVDF powder was completely dissolved, the solution was further treated in an ultrasonic bath for 20 min to ensure that both components were thoroughly mixed. Afterward, the solution was poured into a petri dish with a diameter of 7 cm, which was dried in an oven at 80°C for 3 hours and then heated at 140°C for 16 hours to remove the solvent. After the cast membrane was cooled to room temperature, it was peeled from the petri dish in deionized water. Membranes with Nafion/PVDF ratios of 1:2 and 2:1 were also prepared for comparison.

Lithiation of the Nafion/PVDF membrane

A Nafion/PVDF membrane (3 cm × 3 cm) was first boiled in 0.5 M H_2SO_4 at 80°C for 2 hours and then rinsed in deionized water several times. The resulting membrane was then boiled in 1 M LiOH solution at 80°C for 2 hours to convert it into a Li form. After the resulting membrane was boiled and rinsed in deionized water, it was dried at 80°C overnight. The resulting lithiated membranes with Nafion/PVDF ratios of 1:1, 1:2, and 2:1 were named as NP11, NP12, and NP21, respectively. The DL of the membrane was calculated with the following equation

$$\mathrm{DL} = \frac{W_2 - W_1}{W_1} \times 100\%$$

where W_1 and W_2 are the weight of the dry membrane before and after lithiation, respectively.

RFLB full cell assembly

For the RFLB full cell used in the charge-discharge tests, carbon felt and nickel foam served as cathodic and anodic electrodes, respectively. The

active area of the electrode was 4 cm^2. The catholyte and anolyte consisted of 5 mM Fc and 5 mM $FcBr_2$ in 1.0 M LiTFSI/TEGDME, and 5 mM $Co(Cp)_2$ and 5 mM $Co(Cp^*)_2$ in 1.0 M LiTFSI/TEGDME, respectively. $LiFePO_4$ (6.4 mg) and TiO_2 (7.0 mg) were used as Li^+ storage materials in cathodic and anodic tanks, respectively.

Electrochemical measurements

All the electrochemical measurements were conducted with a multichannel potentiostat (Metrohm Autolab, PGSTAT302N) in an argon-filled glove box at room temperature. The electrolyte was 1.0 M LiTFSI in TEGMDE. The cyclic voltammetry (CV) tests were carried out with a three-electrode setup, in which a glassy carbon disc electrode was used as the working electrode, whereas lithium foils were used as counter and reference electrodes.

For the galvanostatic charge-discharge test, 1 ml of catholyte and 1 ml of anolyte were used and the cell was tested at a constant current density from 0.05 to 0.0875 mA cm^{-2}. For the GITT test, the volumes of both catholyte and anolyte were 3 ml [catholyte, 5 mM Fc and 5 mM $FcBr_2$ in 1.0 M LiTFSI/TEGDME; anolyte, 5 mM $Co(Cp)_2$ and 5 mM $Co(Cp^*)_2$ in 1.0 M LiTFSI/TEGDME], and five times redox mediator equivalent solid materials were added into the tanks. Before the GITT test, the cell was fully discharged. The GITT measurement was conducted at a cutoff voltage of 2.50 V. The cell was charged at a constant density of 0.05 mA cm^{-2} for 10 s, followed by relaxation at an open-circuit state for 10 s.

SUPPLEMENTARY MATERIALS

Supplementary material for this article is available at http://advances.sciencemag.org/cgi/content/full/1/10/e1500886/DC1

RFLB full cell performance with a lithiated Nafion 212 membrane

Fig. S1. Voltage profiles of an RFLB full cell using the lithiated Nafion 212 membrane.

Swelling and solvent uptake of lithiated Nafion 212 and NP11 membranes

Table S1. Swelling and PC uptake of the lithiated Nafion 212 and NP11 membrane.

Resistance of an RFLB with the NP11 membrane

Fig. S2. Nyquist plots of the impedance of the NP11 membrane measured in an RFLB cell after different durations of electrolyte circulation.

AFM phase image of a lithiated Nafion 212 membrane

Fig. S3. AFM image of a lithiated Nafion 212 membrane for comparison.

Permeability test of redox mediators across different membranes

Fig. S4. Permeability study of the membranes.

Morphological characterization of the NP11 membrane before and after cycling

Fig. S5. Morphological features of the NP11 membrane.

Areal resistance of Nafion and composite membranes

Table S2. Comparison of the areal resistance, conductivity, and DL of different membranes.

Cell performance of an RFLB full cell with the NP21 membrane

Fig. S6. Cell performance of an RFLB with the NP21 membrane.

Fig. S7. Nyquist plots of the impedance of a conductivity cell with different membranes.

AFM image of the NP11 membrane after cycling in an RFLB full cell

Fig. S8. AFM image of the NP11 membrane after cycling in an RFLB full cell.

FTIR spectra of the NP11 membrane before and after cycling in an RFLB full cell

Fig. S9. FTIR spectra of the NP11 membrane before and after cycling in an RFLB full cell.

RFLB full cell performance with the NP11 membrane

Fig. S10. Voltage profiles of the RFLB full cell.

REFERENCES AND NOTES

1. W. Wang, Q. Luo, B. Li, X. Wei, L. Li, Z. Yang, Recent progress in redox flow battery research and development. *Adv. Funct. Mater.* **23**, 970–986 (2013).
2. X. Li, H. Zhang, Z. Mai, H. Zhang, I. Vankelecom, Ion exchange membranes for vanadium redox flow battery (VRB) applications. *Energy Environ. Sci.* **4**, 1147–1160 (2011).
3. M. Skyllas-Kazacos, M. H. Chakrabarti, S. A. Hajimolana, F. S. Mjalli, M. Saleem, Progress in flow battery research and development. *J. Electrochem. Soc.* **158**, R55–R79 (2011).
4. A. Z. Weber, M. M. Mench, J. P. Meyers, P. N. Ross, J. T. Gostick, Q. Liu, Redox flow batteries: A review. *J. Appl. Electrochem.* **41**, 1137–1164 (2011).
5. F. Cheng, J. Liang, Z. Tao, J. Chen, Functional materials for rechargeable batteries. *Adv. Mater.* **23**, 1695–1715 (2011).
6. B. Li, Z. Nie, M. Vijayakumar, G. Li, J. Liu, V. Sprenkle, W. Wang, Ambipolar zinc-polyiodide electrolyte for a high-energy density aqueous redox flow battery. *Nat. Commun.* **10**, 1–8 (2015).
7. B. Hwang, M.-S. Park, K. Kim, Ferrocene and cobaltocene derivatives for non-aqueous redox flow batteries. *ChemSusChem* **8**, 310–314 (2015).
8. J. Mun, M.-J. Lee, J.-W. Park, D.-J. Oh, D.-Y. Lee, S.-G. Doo, Non-aqueous redox flow batteries with nickel and iron tris(2,2′-bipyridine) complex electrolyte. *Electrochem. Solid-State Lett.* **15**, A80–A82 (2012).
9. Q. Liu, A. A. Shinkle, Y. Li, C. W. Monroe, L. T. Thompson, A. E. S. Sleightholme, Non-aqueous chromium acetylacetonate electrolyte for redox flow batteries. *Electrochem. Commun.* **12**, 1634–1637 (2010).
10. A. E. S. Sleightholme, A. A. Shinkle, Q. Liu, Y. Li, C. W. Monroe, L. T. Thompson, Non-aqueous manganese acetylacetonate electrolyte for redox flow batteries. *J. Power Sources* **196**, 5742–5745 (2011).
11. Q. Liu, A. E. S. Sleightholme, A. A. Shinkle, Y. Li, L. T. Thompson, Non-aqueous vanadium acetylacetonate electrolyte for redox flow batteries. *Electrochem. Commun.* **11**, 2312–2315 (2009).
12. B. Huskinson, M. P. Marshak, C. Suh, S. Er, M. R. Gerhardt, C. J. Galvin, X. Chen, A. Aspuru-Guzik, R. G. Gordon, M. J. Aziz, A metal-free organic–inorganic aqueous flow battery. *Nature* **505**, 195–198 (2014).
13. J. Huang, L. Cheng, R. S. Assary, P. Wang, Z. Xue, A. K. Burrell, L. A. Curtiss, L. Zhang, Liquid catholyte molecules for nonaqueous redox flow batteries. *Adv. Energy Mater.* **5**, 1401782–1401788 (2015).
14. Y. Ding, Y. Zhao, G. Yu, A membrane-free ferrocene-based high-rate semiliquid battery. *Nano Lett.* **15**, 4108–4113 (2015).
15. X. Wei, W. Xu, J. Huang, L. Zhang, E. Walter, C. Lawrence, M. Vijayakumar, W. A. Henderson, T. Liu, L. Cosimbescu, B. Li, V. Sprenkle, W. Wang, Radical compatibility with nonaqueous electrolytes and its impact on an all-organic redox flow battery. *Angew. Chem. Int. Ed.* **54**, 1–5 (2015).
16. Y. Zhao, L. Wang, H. R. Byon, High-performance rechargeable lithium-iodine batteries using triiodide/iodide redox couplesin an aqueous cathode. *Nat. Commun.* **4**, 1896–1902 (2013).
17. X. Wei, L. Cosimbescu, W. Xu, J. Z. Hu, M. Vijayakumar, J. Feng, M. Y. Hu, X. Deng, J. Xiao, J. Liu, V. Sprenkle, W. Wang, Towards high-performance nonaqueous redox flow electrolyte via ionic modification of active species. *Adv. Energy Mater.* **5**, 1400678–1400685 (2015).
18. X. Wei, W. Xu, M. Vijayakumar, L. Cosimbescu, T. Liu, V. Sprenkle, W. Wang, TEMPO-based catholyte for high-energy density nonaqueous redox flow batteries. *Adv. Mater.* **26**, 7649–7653 (2014).
19. K. Takechi, Y. Kato, Y. Hase, A highly concentrated catholyte based on a solvate ionic liquid for rechargeable flow batteries. *Adv. Mater.* **27**, 2501–2506 (2015).
20. M. Duduta, B. Ho, V. C. Wood, P. Limthongkul, V. E. Brunini, W. C. Carter, Y.-M. Chiang, Semi-solid lithium rechargeable flow battery. *Adv. Energy Mater.* **1**, 511–516 (2011).
21. T.-S. Wei, F. Y. Fan, A. Helal, K. C. Smith, G. H. McKinley, Y.-M. Chiang, J. A. Lewis, Biphasic electrode suspensions for Li-ion semi-solid flow cells with high energy density, fast charge transport, and low-dissipation flow. *Adv. Energy Mater.* **5**, 1500535–1500541 (2015).
22. H. Chen, Q. Zou, Z. Liang, H. Liu, Q. Li, Y.-C. Lu, Sulphur-impregnated flow cathode to enable high-energy-density lithium flow batteries. *Nat. Commun.* **6**, 5877–5885 (2015).
23. S. Hamelet, T. Tzedakis, J.-B. Leriche, S. Sailler, D. Larcher, P.-L. Taberna, P. Simon, J.-M. Tarascon, Non-aqueous Li-based redox flow batteries. *J. Electrochem. Soc.* **159**, A1360–A1367 (2012).
24. M. Youssry, L. Madec, P. Soudan, M. Cerbelaud, D. Guyomard, B. Lestriez, Non-aqueous carbon black suspensions for lithium-based redox flow batteries: Rheology and simultaneous rheo-electrical behavior. *Phys. Chem. Chem. Phys.* **15**, 14476–14486 (2013).
25. Q. Huang, H. Li, M. Grätzel, Q. Wang, Reversible chemical delithiation/lithiation of $LiFePO_4$: Towards a redox flow lithium-ion battery. *Phys. Chem. Chem. Phys.* **15**, 1793–1797 (2013).
26. F. Pan, J. Yang, Q. Huang, X. Wang, H. Huang, Q. Wang, Redox targeting of anatase TiO_2 for redox flow lithium-ion batteries. *Adv. Energy Mater.* **4**, 1400567–1400573 (2014).
27. X. Xu, Z. Wen, X. Yang, J. Zhang, Z. Gu, High lithium ion conductivity glass-ceramics in Li_2O–Al_2O_3–TiO_2–P_2O_5 from nanoscaled glassy powders by mechanical milling. *Solid State Ion.* **177**, 2611–2615 (2006).
28. Y. Zhao, Y. Ding, J. Song, G. Li, G. Dong, J. B. Goodenough, G. Yu, Sustainable electrical energy storage through the ferrocene/ferrocenium redox reaction in aprotic electrolyte. *Angew. Chem. Int. Ed.* **53**, 11036–11040 (2014).
29. C. Sun, S. Rajasekhara, J. B. Goodenough, F. Zhou, Monodisperse porous $LiFePO_4$ microspheres for a high power Li-ion battery cathode. *J. Am. Chem. Soc.* **133**, 2132–2135 (2011).
30. Z. Yang, J. Zhang, M. C. W. Kintner-Meyer, X. Lu, D. Choi, J. P. Lemmon, J. Liu, Electrochemical energy storage for green grid. *Chem. Rev.* **111**, 3577–3613 (2011).

31. C. Jia, Y. Cheng, X. Ling, G. Wei, J. Liu, C. Yan, Sulfonated poly(ether ether ketone)/functionalized carbon nanotube composite membrane for vanadium redox flow battery applications. *Electrochim. Acta* **153**, 44–48, (2015).
32. A. M. Affoune, A. Yamada, M. Umeda, Surface observation of solvent-impregnated Nafion membrane with atomic force microscopy. *Langmuir* **20**, 6965–6968 (2004).
33. J. R. Jennings, Q. Huang, Q. Wang, Kinetics of Li_xFePO_4 lithiation/delithiation by ferrocene-based redox mediators: An electrochemical approach. *J. Phys. Chem. C*, **119**, 17522–17528 (2015).
34. E. Ventosa, M. Skoumal, F. J. Vázquez, C. Flox, J. R. Morante, Operando studies of all-vanadium flow batteries: Easy-to-make reference electrode based on silver–silver sulfate. *J. Power Sources* **271**, 556–560 (2014).

Acknowledgments
Funding: This work is supported by the National Research Foundation, Prime Minister's Office, Singapore, under its Competitive Research Program (CRP award no. NRF-CRP8-2011-04). **Author contributions:** Q.W. conceived the idea and supervised the work. C.J. designed and synthesized the membranes and performed most of the experiments. C.J. and Y.G.Z. studied the general properties of the membranes. F.P. conducted CV and full cell measurements with the Nafion 212 membrane. L.L. and Q.H. provided $LiFePO_4$ material and made the granules. C.J., F.P., and Q.W. wrote the report. **Competing interests:** The authors declare that they have no competing interests. **Data and materials availability:** All data needed to evaluate the conclusions in the paper are present in the paper and/or the Supplementary Materials. Additional data related to this paper may be requested from the authors.

Submitted 6 July 2015
Accepted 19 October 2015
Published 27 November 2015
10.1126/sciadv.1500886

Citation: C. Jia, F. Pan, Y. G. Zhu, Q. Huang, L. Lu, Q. Wang, High–energy density nonaqueous all redox flow lithium battery enabled with a polymeric membrane. *Sci. Adv.* **1**, e1500886 (2015).